CrossMark

RESEARCH PAPER

Investigation of membrane fouling at the microscale using isopore filters

Majid Ebrahimi Warkiani · Filicia Wicaksana · Anthony Gordon Fane · Hai-Qing Gong

Abstract Investigations of membrane fouling at the pore-scale have long been of limited interest due to microstructural defects of the commercial membranes that prevent any quantitative analysis of the experimental results. In this paper, we employed novel microengineered membranes with regular pore size to investigate the effect of the membrane pore geometry on the fouling mechanisms during filtration of micron-sized particles. For particles larger than the membrane pore size, the fouling mechanism was pore blockage followed by the cake filtration, while pore narrowing was the dominant mechanism when particles were smaller than the membrane pore size. Filtration with the slotted pore membrane offers some interesting advantages comparing to the filtration with circular pores. The rate of flux decline was slower for the membrane with slotted pores compared with the membrane with circular pores since the initial particle deposition only covered a small fraction of the pores. It was also found that the flow resistance of the slotted pore membrane is much lower than the circular one because a slotted pore has a smaller perimeter than several circular pores with the same total surface area. We can conclude that by proper selection of membrane pore geometry, flux decline can be hindered while maintaining a high selectivity during microfiltration. These findings can be useful also for researchers who are using microfluidic platforms with integrated isopore filters for various applications such as stem cell enrichment, cancer cell isolation, blood fractionation and pathogen removal.

Keywords Isopore membrane · Filtration · Fouling · Microfluidics · MEMS

M. E. Warkiani (✉)
School of Mechanical and Manufacturing Engineering,
Australian Center for NanoMedicine, University of New South
Wales, Sydney NSW 2052, Australia
e-mail: m.warkiani@unsw.edu.au

F. Wicaksana · A. G. Fane
Singapore Membrane Technology Centre (SMTC),
Singapore, Singapore

Present Address:
F. Wicaksana
Department of Chemical and Materials Engineering,
University of Auckland, Auckland, New Zealand

A. G. Fane
School of Civil and Environmental Engineering,
Nanyang Technological University, 50 Nanyang Avenue,
Singapore 637723, Singapore

H.-Q. Gong
School of Mechanical and Aerospace Engineering,
Nanyang Technological University, 50 Nanyang Avenue,
Singapore 639798, Singapore

1 Introduction

The separation of micron-sized particles from an aqueous solution using a synthetic membrane is an important operation in many chemical and biological processes such as drug discovery (Giacomini et al. 2010), circulating tumor cells (CTCs) isolation (Coumans et al. 2013), pathogen detection (Warkiani et al. 2011a), chromatography (Sano et al. 2003) and blood fractionation (Ji et al. 2008). During a membrane separation process, the particles retained on the feed side (retentate) start to accumulate near the membrane surface, and consequently, the concentration of particles becomes higher near the membrane than in the bulk retentate. This phenomenon is called concentration polarization, which is a major obstacle in the widespread application of membranes (Fane and Fell 1987; Baker 2004).

Springer

Over the past decades, various studies shown that membrane fouling is controlled by a complex interplay between particles and hydrodynamic forces acting on them (Bacchin et al. 1995; Iscan et al. 2007). In addition, previous studies demonstrated that the membrane pore morphology could have a considerable effect on the rate of flux decline and fouling mechanism (Kuiper et al. 2002b; Bromley et al. 2002; Kuiper et al. 1998). However, investigations of membrane fouling at the pore-scale have long been of limited interest due to microstructural defects of the commercial membranes (i.e., rough surfaces, tortuous pore paths and batch to batch variations) that prevent any quantitative analysis of the experimental results (Lin et al. 2009; Bacchin et al. 2011; Chen et al. 2010).

Recent developments in micro/nanotechnology have provided novel techniques for controlling the detailed microstructure of membrane materials, allowing the fabrication of membranes with precise pores and shapes (Warkiani et al. 2011c, 2012). Over the past decade, micro-/nano-engineered membranes with regular pores have been deployed extensively for variety of applications such as virus filtration (Yang et al. 2006), water purification (Jackson and Hillmyer 2010), bacteria detection (Warkiani et al. 2011b), DNA/protein separation (Venkatesan et al. 2009) or even stencil for cell patterning (Wright et al. 2008). A comprehensive overview of these membranes and their applications has been reviewed recently by Warkiani et al. (2013). In this study, we employed isopore filters with different pore geometries (i.e., circular and slotted) as a new platform for investigation of membrane fouling at the pore-scale in order to demonstrate another application of them. These membranes were used to determine the rate of flux decline at various particle concentrations and also study the effect of membrane pore geometry on the fouling mechanism by post-SEM and direct observation analysis. The observations were validated by analysis of the filtration data using the available classical filtration models for this purpose. The results clearly show the importance of the membrane pore morphology on the initial flux decline, flow resistance and on the transition to cake filtration mechanism on the surface of isopore microengineered membranes.

2 Materials and methods

2.1 Fabrication of isopore membranes

Figure 1a schematically shows the process for fabrication of isopore microengineered membranes. The microfabrication process begins with deposition of a 200-nm-thin Cr/Cu layer onto a 4-inch silicon wafer using a magnetron sputtering machine. The chrome layer serves as the conducting seed layer for electroplating. Afterward, a 10-µm-thick

AZ9260 (Microchemicals GmbH) photoresist was spin-coated on the wafer and photolithography was carried out by a Karl Suss MA6 mask aligner (Karl Suss Inc.). Then, the exposed film was developed at the room temperature in the AZ 400 k (Microchemicals GmbH) developer for 2 min with manual agitation. Next, the seed layer was connected to a negative electrode and then electroplated using a sulfuric-based nickel electroplating solution. To avoid over-plating, the height of the electroplated nickel was kept to less than that of the patterned photoresist. Finally, the isopore membrane was achieved by dissolving the photoresist and seed layer inside acetone and Cu etchant (Sigma-Aldrich), respectively. The obtained membranes had a pore dimension (diameter or slit width) of 3 ± 0.05 µm and thickness of 8 ± 0.1 µm. The slotted pore membrane had a pore length of 8 µm and a porosity of approximately 32 %, while this value is around 30 % for the circular pore membrane. Figure 1a also shows SEM images of the metallic isopore membranes with circular and slotted openings.

2.2 Preparation of latex suspension

White polystyrene latex particles with diameters of 1, 3 and 6 µm (CV < 5 %) were obtained from Sigma-Aldrich (Sigma-Aldrich®). Feed solutions were prepared by diluting the stock solution with ultra-pure water (18.2 MΩ cm) from a Millipore purification unit (MilliQ plus). The latex stock suspension was sonicated for 2 min in an ultrasonic bath before each test, and the suspension was kept homogenous by stirring the solution with a magnetic stirrer during experiments.

2.3 Experimental setup

The microfiltration experiments were performed in both crossflow and dead-end modes. The crossflow module was designed and fabricated from PMMA (Polymethyl methacrylate) by laser cutting and thermal bonding (Fig. 1c). The effective membrane area and height of the crossflow channel was 6.25×10^{-4} m² and 0.0015 m, respectively. The clean water permeability of the membranes was measured in the pressure range of 5–20 kPa at 20 °C. The average clean water permeability of the circular pore membrane was around 0.38×10^6 L/m²hbar, while this value was around 2×10^6 L/m²hbar for the slotted membrane. This is a difference of 5× in favor of the slotted membrane, which is discussed below. A schematic representation of the experimental setup used in this study is shown in Fig. 1b. Direct observation of particle deposition on the membrane surface was also performed with a Zeiss microscope and a CCD camera during microfiltration tests. The microengineered membranes were glued onto a plastic mesh with 600 µm openings to enhance their mechanical strength
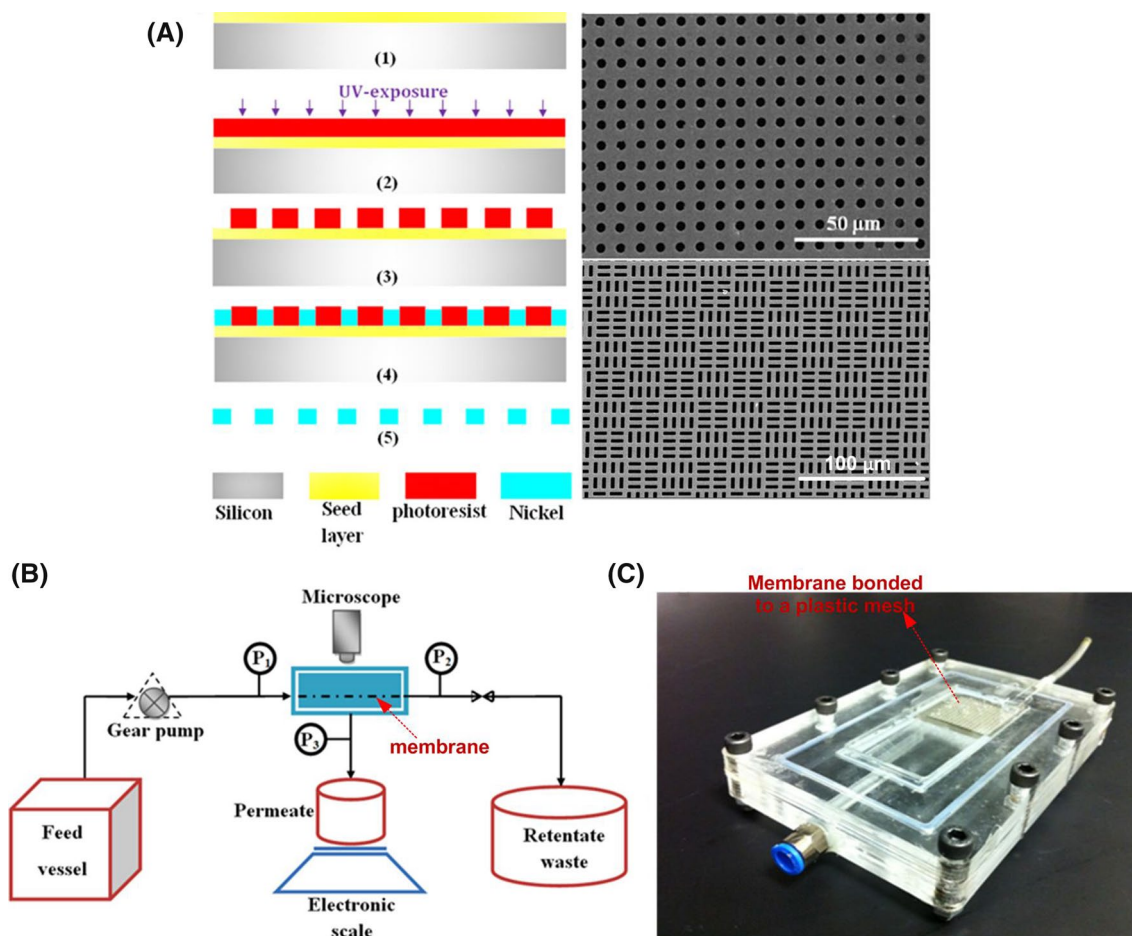
Fig. 1 a *Left* The fabrication process of the isopore membranes: (*1*) deposition of the seed layer (Cr/Cu) on a Si substrate, (*2*) spin-coating of a thick layer of AZ9260 on the Si wafer and UV exposure through a mask, (*3*) development of the exposed film inside the AZ developer, (*4*) electroplating of the Ni between photoresist pillars, and (*5*) releasing the isopore membrane by dissolving the photoresist and seed layer in acetone and Cu etchant, respectively. **a** *right* SEM image of a circular pore membrane (3 μm diameter), and SEM image of a slotted pore membrane (3 μm slit width). **b** Schematic representation of the experimental setup used for the tests. **c** Optical image of the crossflow module fabricated from PMMA by laser cutting technique

(Ebrahimi Warkiani et al. 2012). Prior to the experiments, all the membranes were inspected under an optical microscope to check their integrity. Subsequently, they were pre-wetted with pure water for 5 min. Our dead-end microfiltration setup is described in details in a recent publication of our group (Taheri et al. 2013).

2.4 Blocking model

In order to describe the blocking phenomena during microfiltration with latex particles, the Hermans and Bredee's blocking model (Hermans and Bredée 1936), which describes the relationship between the filtrate volume and the filtration time, has been used:

$$\frac{\mathrm{d}^2 t}{\mathrm{d}v^2} = k \left(\frac{\mathrm{d}t}{\mathrm{d}v} \right)^i$$

where t is the filtration time, v is the filtrate volume, and the index i and the constant k are depend on the blocking models. In this equation, $i = 2, 1.5, 1$ and 0 apply to the complete blocking, standard blocking, intermediate blocking and cake filtration models, respectively (Hermans and Bredée 1936). It should be noted that this model is a single pore blocking model which is rarely a good description of a filtration process. Combined pore blocking and cake filtration models have also been developed (Duclos-Orsello et al. 2006) which can be employed for the complex conditions where several mechanisms are involved.

2.5 Integrity test with bubble point technique

We employed the bubble point test for integrity testing of the isopore microengineered membranes. The relationship between the minimum pressure (ΔP) to be applied on the

liquid to enter the pores of a membrane is given by the Laplace–Young equation (Baker 2004) as follows:

$$\Delta P = \frac{-2\gamma_L \cos\theta}{r}$$

where γ_L is the surface tension of the liquid, θ is the contact angle of the liquid with the surface and r is the membrane pore radius. This equation was employed to estimate the bubble point of the isopore membranes. For this purpose, the surface treated microfilters were immersed in isopropanol ($\gamma = 21.7 \times 10^{-3}$ N/m) for 5 min and bubble point tests were carried out by applying pressure beneath the membrane in a fabricated test rig. The measured values of the bubble point for the microengineered membrane were compared with those obtained from the Laplace–Young equation. If the measured pressure was 10–15 % lower than the calculated one, the microengineered membrane was discarded assuming it had defects.

3 Results and discussion

Understanding of mechanisms that lead to the formation of fouling layers is a key point to optimize process performance during filtration of micron size particles. For this purpose, it is necessary to have a direct access to the experimental information at the pore-scale during microfiltration. Microfiltration with different particles sizes can reveal how a pore is blocked and how the performance of a membrane will change as a function of feed's concentration and global variation of operating conditions. To unveil another application of the isopore membranes, we have employed them in this study as an ideal platform for investigation of membrane fouling at the pore-scale using latex particles of different sizes and concentrations as a model feed for microfiltration. Direct observation of the latex deposition on the membrane was utilized to reveal the mechanism of membrane pore blockage. When the pore and particle sizes are known and the experimental conditions are similar (i.e., feed rate, temperature, membrane's material, porosity, thickness), the mechanism for particle deposition can also be determined and compared with available analytical models (Bromley et al. 2002; Hwang and Lin 2002; Gironès 2005).

3.1 Microfiltration with particles smaller than the pore size

To evaluate the performance of the isopore microengineered membranes, latex suspensions containing 1 μm particles at two different concentrations (0.1 and 1 g/L) were tested. The goal was to determine the flux decline rate as a function of particle concentration. The membrane blockage was also studied by analysis of microscopic and SEM

images after microfiltration. The filtrations were performed in dead-end mode at a constant pressure of 20 kPa for both circular and slotted pore membranes, and the permeate volume was measured over time. The constant pressure during the dead-end filtration was obtained by supplying pressure-regulated air to a sealed solution reservoir that was connected to the membrane modules (Taheri et al. 2013). The results are expressed as normalized flux (i.e., J/J_w), where J is the recorded flux from the experiments, and J_w is the flux obtained from the tests with ultra-pure water. Figure 2a, b shows the results for a circular pore membrane with a 3-μm pore size. It can be seen that a severe flux decline occurred with a more concentrated feed, producing a permeated volume of only 75 mL during 30 min of filtration. For the diluted feed (0.1 g/L), the flux decline occurred more gradually. This is because at the higher concentrations, the chance that particles meet and block the pore becomes larger, thus decreasing the flux in time. Since the particles are smaller than the membrane pores, a few particles can deposit on the membrane surface, while the remainder are carried by the filtrate, entering and plugging the membrane pores. Due to the high transmembrane pressure (TMP), particles mostly come into contact with the pore walls. At this condition, particles normally started to deviate from the major streamlines, and therefore, particles could be adsorbed to the pore walls (Bacchin et al. 2011; Brans et al. 2007).

Figure 2c shows the flux comparison of the circular and slotted pore membranes for the filtration of latex suspension with a concentration of 1 g/L. It can be seen that the slotted pore membrane gives a higher flux, and therefore, a larger collected volume than the circular pore membrane, presenting its better performance. A remarkable decrease in the flux of circular pore membrane is mainly due to the rapid particle deposition (i.e., bridging) inside the pores, leading to the significant reduction of the collected volume. Since the rate of TMP changes is lower for the slotted pore membrane particles normally follow the major streamlines, resulting in minimal adsorption and blocking. In order to evaluate the experimental results with Herman's model (Hermans and Bredée 1936), the slope of the logarithmic plot of d^2t/dV^2 versus dt/dV (i.e., i value) was calculated as 1.55 ± 0.02 for the circular pore and 1.60 ± 0.07 for the slotted pore membrane, indicating that the main fouling mechanism is more likely to be standard blocking or pore narrowing. Post-filtration SEM analysis of the samples revealed that blocking has occurred within the membrane pores (see Fig. 2d, e). It can be seen that up to three particles of 1 μm can block a single circular pore, while for the slotted pore membrane, shown in Fig. 2d, a relatively large open area is still available for water to penetrate although several particles have been deposited inside the pore. Our observations are in good agreement with the
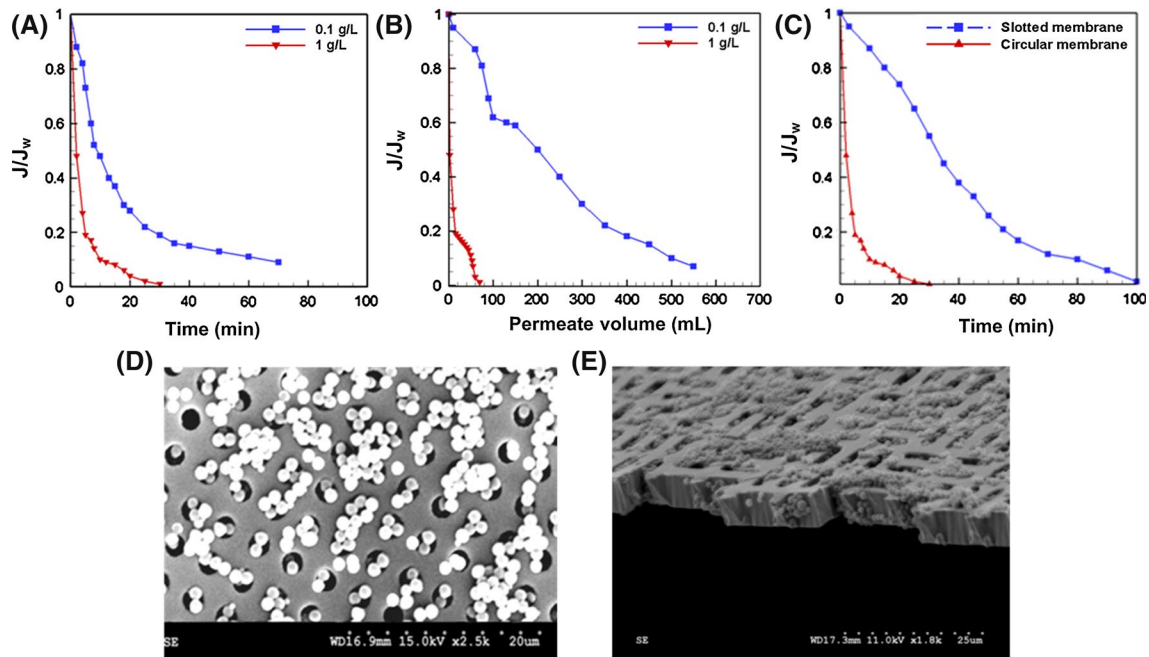
Fig. 2 Normalized flux of two different latex solution concentrations as a **a** function of time, and **b** permeated volume for a circular pore membrane with 3 μm pore size. **c** Normalized flux versus time for the circular and slotted pore membrane. The concentration of the solution was 1 g/L for the experiments and pressure was 20 kPa. SEM images of two isopore microengineered filters, **d** circular pore and **e** slotted pore with deposited latex particles after microfiltration of latex particles of 1 μm size. Note that particles may have been displaced or removed in some regions during sample preparation of electron microscopy

results of previous studies (Lin et al. 2009; Bacchin et al. 2011; Brans et al. 2007; Ramachandran and Fogler 1999) that investigated the transport of particles through isopore track-etched membranes.

3.2 Microfiltration with particles equal to the pore size

Filtration tests with 3 μm diameter particles were also performed to examine how particles with a similar size to the membrane pores would deposit on the membrane surface. Experiments were performed in the dead-end mode with various feed concentrations similar to those described in the Sect. 3.1. Microfiltration results (i.e., normalized flux vs. time and permeate volume) showed that a very rapid flux decline took place within a couple of minutes for high-concentration suspensions, until a steady-state condition was achieved resulting in a very low permeate flux (data not shown). Since the cake formed by the latex particles is not completely dense, water can still penetrate through the microvoids between particles and a residual flux can be measured.

Figure 3a shows a flux comparison of the circular and slotted pore membranes. The flux decline data were consistent with an initial fouling mechanism due to intermediate blockage followed by cake filtration for both membranes. The initial rate of flux decline was slower for the membrane with slotted pores compared with the membrane with circular pores since the initial particle deposition only covered a fraction of the slotted pore area. Figure 3b depicts the total resistance obtained from the flux data shown in Fig. 3a. For the slotted pore membrane, the flow resistance is much smaller than the circular one because a slotted pore has a smaller perimeter than several circular pores with the same total surface area (i.e., if the ratio of slit length to the slit width be larger than 3). Hence, this smaller perimeter gives less flow resistance. This behavior has been also reported by other researchers for the case of commercial membranes (Bromley et al. 2002; Kuiper et al. 2002a; Warkiani and Gong 2014). Figure 3b also shows that the total resistance curves have a concave down trend suggesting fouling by the pore blockage and cake filtration (Dubitsky et al. 2002). SEM photos token after microfiltration from the surface of isopore membranes also shown in Fig. 3c, d. In this case, the slope of the logarithmic plot of d^2t/dV^2 versus dt/dV for the circular pore membrane was around 1.1 ± 0.1 for the initial stage of filtration indicating the intermediate pore blockage condition followed by a zero slope on the log–log plot, consistent with the classical cake filtration model.

3.3 Microfiltration with particles bigger than the pore size

For comparison with the previous cases, we also examined how particles with a larger diameter than then membrane

Fig. 3 **a** Normalized flux versus time for the circular and slotted pore membrane during microfiltration of 3 μm size particles. **b** Total resistance of each membrane calculated based on microfiltration data obtained during experiments. The concentration of the solution was 1 g/L for all the experiments and pressure was 20 kPa. **c** and **d** SEM images depicting surface of microengineered membranes after microfiltration of particles equal to the pore size (3 μm). Note that particles may have been displaced or removed in some regions during sample preparation of electron microscopy
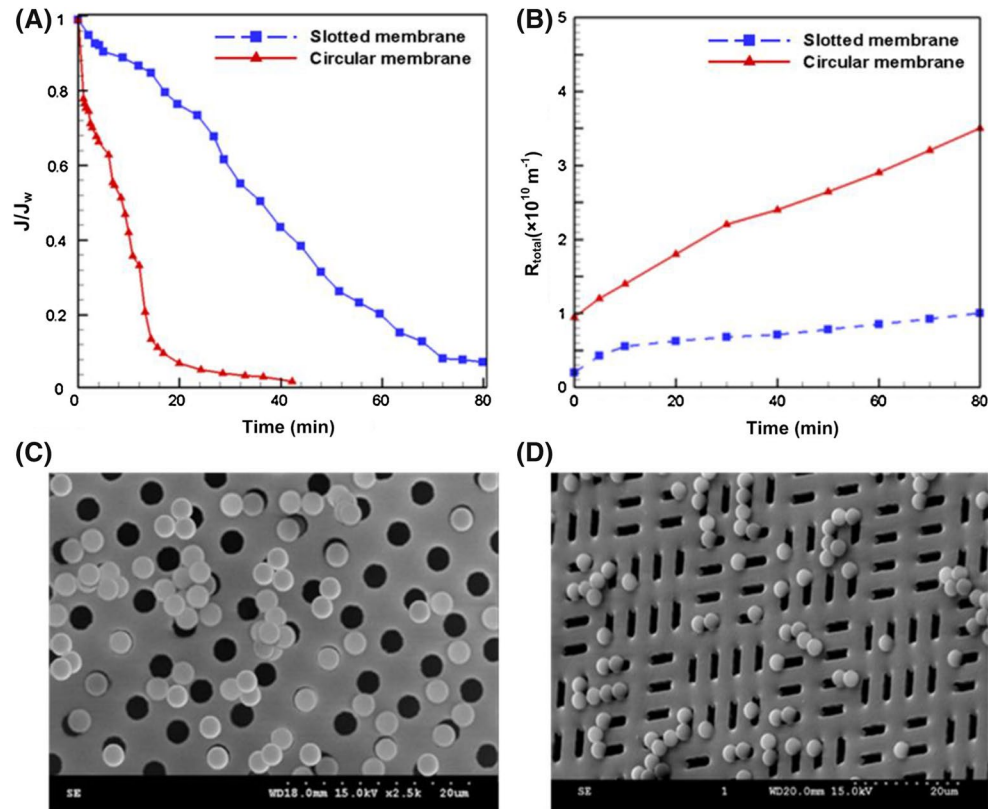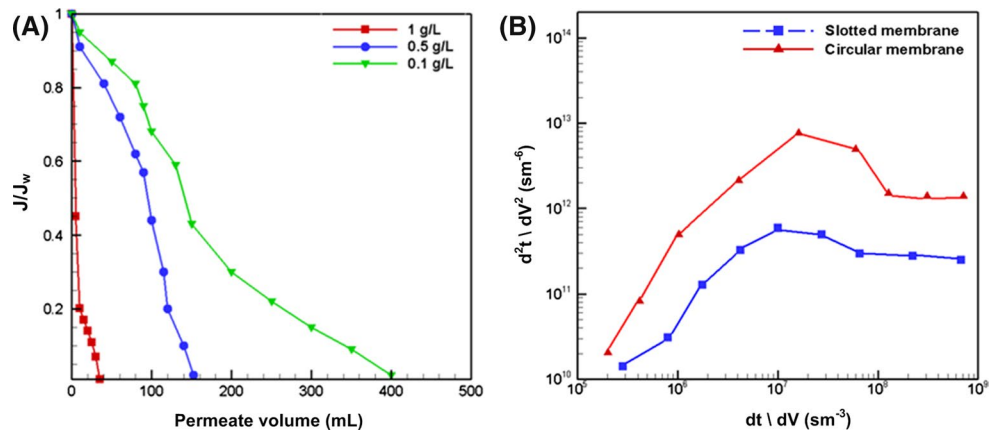

Fig. 4 **a** Normalized flux versus permeated volume during microfiltration of 6 μm latex particles with different concentrations for a circular pore membrane, **b** derivative plot for 6 μm latex filtration (0.1 g/L) through the circular and slotted pore membrane under 20 kPa pressures in dead-end mode

pore size (6 μm) would deposit on the membrane's surface and cause pore blockage and subsequent fouling. For both membranes, the microfiltration was performed with various feed concentrations under 20 kPa pressure in dead-end mode. Figure 4a shows typical normalized flux data versus filtration volume for 6 μm latex particles at three different concentrations. It can be seen that rate of flux decline for the most concentrated feed (i.e., 1 g/L) is much more severe than two others, producing a permeated volume of only 37 mL during filtration while this value is around 150 and 400 mL for the feed with concentration of 0.5 and 0.1 g/L, respectively. A better picture of the fouling mechanism

during filtration of 6 μm latex particles through circular and slotted pore membranes was achieved using the log–log plot as shown in Fig. 4b. The derivative plot for the circular pore membrane shows an initial slope of 2 ± 0.05, which is similar to the prediction of Herman's pore blockage model. The slope of d^2t/dV^2 versus dt/dV approaches a value of zero for long filtration times (i.e., large value of dt/dV), consistent with classical cake filtration model (Ho and Zydney 1999; Chandler and Zydney 2006). The almost linear behavior of normalized flux versus filtration volume (Fig. 4a) also confirmed that pore blockage is the dominant mechanism at the early stage of filtration (Ho and Zydney
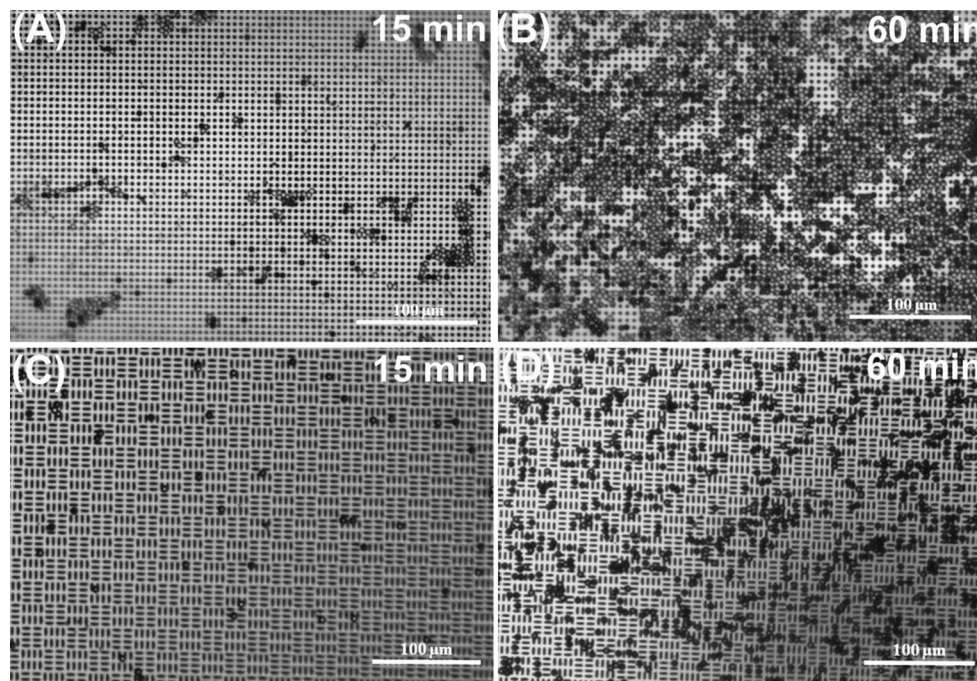
Fig. 5 Optical images of particle deposition during the filtration of 6 μm latex particles (0.1 g/L) at CFV = 0.2 m/s, **a** and **b** on a circular pore membrane, and **c** and **d** on a slotted pore membrane at imposed flux of 100 L/m² h

2002). For the slotted pore membrane, a single 6-μm particle cannot cover a pore completely; therefore, the fluid can still partially flow through the open (uncovered) region of the pore (i.e., analysis of SEM images also confirmed this). By continuing the filtration, the latex particles will begin to cover all the open areas causing a rapid flux decline during the final stages of the filtration. The derivative data for the slotted pore membrane show a small region with slope of 1.25 ± 0.4 initially (i.e., intermediate pore blockage) followed by another small region with slope of 2.1 ± 0.5 (i.e., pore blockage) and finally, a constant value for the d^2t/dV^2 (i.e., zero slope) for the rest of filtration.

The experiments were also performed under crossflow mode with 0.1 g/L suspension to visualize the mechanism of cake formation on the surface of microengineered membranes. Online observation of the membrane surface during filtration confirmed that all the latex particles were retained on the membrane surface resulting in external fouling for both membranes. Figure 5 shows optical microscopic images of the membranes surface during microfiltration with 6 μm latex particles for around 60 min under equal operating conditions. The crossflow velocity (CFV) was 0.2 m/s and the imposed flux was around 100 L/m² h. Analysis of the images captured during the filtrations of the latex particles revealed that surface coverage for the circular pore membrane was higher than the slotted pore membrane (i.e., 30 % more), indicating that imposed flux was above the critical flux for the circular pore membrane.

It should be noted that the rate of particles deposition and TMP changes was not significant for the slotted pore membrane (see Fig. 5c, d), representing subcritical condition for this membrane. Hence, under these operating conditions, the critical flux of the slotted pore membrane was higher than that of the circular pore membrane. One explanation of the above finding is that for the circular pore membrane, the local changes in water flux are normally happened by the complete blockage of some pores (i.e., deposition of 6-μm latex particles) in contrast to the slotted pore membrane. When operating at constant flux [i.e., critical flux determination involved operation with a series of flux steps (Zhang et al. 2006)], this blockage induces an increase in flux through the unblocked pores consequently. Thus, due to the heterogeneity of the permeate flux, the critical conditions for particle deposition near the membrane surface can be met locally, even if the mean conditions are subcritical when considering the membrane as a homogeneous porous surface (Ognier et al. 2002).

The critical flux of both membranes as a function of crossflow velocity and concentration was also measured and summarized in Fig. 6. It can be seen that (Fig. 6a) by increasing the crossflow velocity, the critical flux for both membranes increased, which is in line with previous studies (Li et al. 1998). Figure 6b shows the critical flux of 6 μm latex particles at different concentrations for the slotted and circular pore membrane. The overall trends were consistent with other researchers' findings that the critical
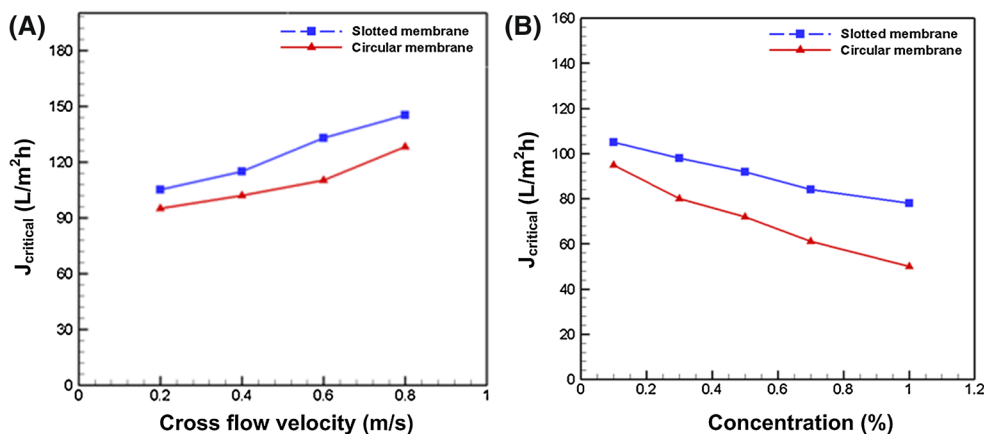
flux decreases with increasing concentration. However, it was observed that rate of critical flux decline for circular pore membrane was slightly higher.

4 Conclusions

Prediction of membrane fouling during filtration of micron size particles remains a difficult step to optimize separation processes. Previous investigations have been devoted toward analysis of global variation of operating conditions such as flow rate and transmembrane changes during microfiltration, while recent studies are deviated toward analysis of particulate fouling at the pore-scale to get better insight about the mechanism of fouling. In this study, we demonstrate the benefit of isopore microengineered membranes with identical pore sizes as a promising tool for studying fouling phenomena for different pore geometries. By employing them, we could successfully study the mechanism of particle deposition at the pore-scale using latex particles. The observations were validated by analysis of the filtration data using the available classical filtration models for this purpose. The obtained results in this study reveal the considerable effects of the pore morphology on the performance of membrane during filtration of micron size particles. Experimental data for latex particles filtration smaller than the pore size show that pore narrowing and cake formation are the dominant mechanisms during filtration. For the particles equal to or larger than the pore size, the flux decline data were consistent with initial fouling by intermediate blockage followed by cake filtration. The initial rate of flux decline was significantly lower for membranes with slotted pores compared with membranes with circular pores since the initial particle deposition only partially covered the slotted holes. These results confirm that slotted pores are less likely to suffer from hydrodynamic particle bridging on the pores and are intrinsically less prone to fouling and easier to clean. It was also found that the flow resistance of the slotted pore

membrane is much lower than the circular one because a slotted pore has a smaller perimeter than several circular pores with the same total surface area. Furthermore, cross-flow microfiltration tests also revealed that the critical flux of the slotted pore membrane is higher than the circular one under equal operating conditions. We can conclude that by proper selection of membrane pore geometry, flux decline can be hindered while maintaining a high selectivity during microfiltration. Moreover, we have shown that microengineered membranes are excellent candidates for the experimental verification of filtration models. Their identical properties such as smooth surface and uniform pore distribution give low particle adhesion and reproducible results.

References

Bacchin P, Aimar P, Sanchez V (1995) Model for colloidal fouling of membranes. AIChE J 41(2):368–376
Bacchin P, Marty A, Duru P, Meireles M, Aimar P (2011) Colloidal surface interactions and membrane fouling: investigations at pore scale. Adv Colloid Interface Sci 164(1):2–11
Baker RW (2004) Membrane technology and applications, 2nd edn. Wiely, New York
Brans G, van Dinther A, Odum B, Schroën C, Boom R (2007) Transmission and fractionation of micro-sized particle suspensions. J Membr Sci 290(1–2):230–240
Bromley A, Holdich R, Cumming I (2002) Particulate fouling of surface microfilters with slotted and circular pore geometry. J Membr Sci 196(1):27–37
Chandler M, Zydney A (2006) Effects of membrane pore geometry on fouling behavior during yeast cell microfiltration. J Membr Sci 285(1–2):334–342
Chen L, Warkiani ME, Liu H-B, Gong H-Q (2010) Polymeric microfilter manufactured by a dissolving mold technique. J Micromech Microeng 20(7):075005
Coumans FA, van Dalum G, Beck M, Terstappen LW (2013) Filter characteristics influencing circulating tumor cell enrichment from whole blood. PLoS ONE 8(4):e61770

Dubitsky A, DeCollibus D, Ortolano GA (2002) Sensitive fluorescent detection of protein on nylon membranes. J Biochem Biophys Methods 51(1):47–56

Duclos-Orsello C, Li W, Ho CC (2006) A three mechanism model to describe fouling of microfiltration membranes. J Membr Sci 280(1–2):856–866

Fane A, Fell C (1987) A review of fouling and fouling control in ultrafiltration. Desalination 62:117–136

Giacomini KM, Huang SM, Tweedie DJ, Benet LZ, Brouwer KLR, Chu X, Dahlin A, Evers R, Fischer V, Hillgren KM (2010) Membrane transporters in drug development. Nat Rev Drug Discovery 9(3):215–236

Gironès M (2005) Inorganic and polymeric microsieves, strategies to reduce fouling. PhD Dissertation, University of Twente, Enschede, The Netherlands, vol 199, issue number 1–2, pp 41–52

Hermans P, Bredée H (1936) Principles of the mathematical treatment of constant-pressure filtration. J Soc Chem Ind 55:1T–4T

Ho CC, Zydney AL (1999) Effect of membrane morphology on the initial rate of protein fouling during microfiltration. J Membr Sci 155(2):261–275

Ho CC, Zydney AL (2002) Transmembrane pressure profiles during constant flux microfiltration of bovine serum albumin. J Membr Sci 209(2):363–377

Hwang KJ, Lin TT (2002) Effect of morphology of polymeric membrane on the performance of cross-flow microfiltration. J Membr Sci 199(1–2):41–52

Iscan AG, Civan F, Kok MV (2007) Alteration of permeability by drilling fluid invasion and flow reversal. J Petrol Sci Eng 58(1):227–244

Jackson EA, Hillmyer MA (2010) Nanoporous membranes derived from block copolymers: from drug delivery to water filtration. ACS Nano 4(7):3548–3553

Ji HM, Samper V, Chen Y, Heng CK, Lim TM, Yobas L (2008) Silicon-based microfilters for whole blood cell separation. Biomed Microdevices 10(2):251–257

Kuiper S, Van Rijn CJM, Nijdam W, Elwenspoek MC (1998) Development and applications of very high flux microfiltration membranes. J Membr Sci 150(1):1–8

Kuiper S, Brink R, Nijdam W, Krijnen G, Elwenspoek M (2002a) Ceramic microsieves: influence of perforation shape and distribution on flow resistance and membrane strength. J Membr Sci 196(2):149–157

Kuiper S, Van Rijn C, Nijdam W, Raspe O, Van Wolferen H, Krijnen G, Elwenspoek M (2002b) Filtration of lager beer with microsieves: flux, permeate haze and in-line microscope observations. J Membr Sci 196(2):159–170

Li H, Fane A, Coster H, Vigneswaran S (1998) Direct observation of particle deposition on the membrane surface during crossflow microfiltration. J Membr Sci 149(1):83–97

Lin J, Bourrier D, Dilhan M, Duru P (2009) Particle deposition onto a microsieve. Phys Fluids 21:073301

Ognier S, Wisniewski C, Grasmick A (2002) Characterisation and modelling of fouling in membrane bioreactors. Desalination 146(1–3):141–147

Ramachandran V, Fogler HS (1999) Plugging by hydrodynamic bridging during flow of stable colloidal particles within cylindrical pores. J Fluid Mech 385:129–156

Sano T, Iguchi N, Iida K, Sakamoto T, Baba M, Kawaura H (2003) Size-exclusion chromatography using self-organized nanopores in anodic porous alumina. Appl Phys Lett 83:4438

Taheri AH, Sim LN, Haur CT, Akhondi E, Fane AG (2013) The fouling potential of colloidal silica and humic acid and their mixtures. J Membr Sci 433:112–120

Venkatesan BM, Dorvel B, Yemenicioglu S, Watkins N, Petrov I, Bashir R (2009) Highly sensitive, mechanically stable nanopore sensors for DNA analysis. Adv Mater 21(27):2771–2776

Warkiani M, Gong H (2014) Micro-fabricated membranes with regular pores for efficient pathogen removal. In: The 15th international conference on biomedical engineering, 2014. Springer, Berlin, pp 424–427

Warkiani ME, Chen L, Lou CP, Liu HB, Rui Z, Gong HQ (2011a) Capturing and recovering of *Cryptosporidium parvum* oocysts with polymeric micro-fabricated filter. J Membr Sci 369:560–568

Warkiani ME, Lou C-P, Gong H-Q (2011b) Fabrication of multi-layer polymeric micro-sieve having narrow slot pores with conventional ultraviolet-lithography and micro-fabrication techniques. Biomicrofluidics 5:036504

Warkiani ME, Lou CP, Gong HQ (2011c) Fabrication and characterization of a microporous polymeric micro-filter for isolation of *Cryptosporidium parvum* oocysts. J Micromech Microeng 21:035002

Warkiani ME, Gong HQ, Fane A (2012a) Surface modification of micro/nano-fabricated filters. Key Eng Mater 508:87–98

Warkiani ME, Lou CP, Liu HB, Gong HQ (2012) A high-flux isopore micro-fabricated membrane for effective concentration and recovering of waterborne pathogens. Biomed Microdevices 14:1–9

Warkiani ME, Bhagat AAS, Khoo BL, Han J, Lim CT, Gong HQ, Fane AG (2013) Isoporous micro/nanoengineered membranes. ACS Nano 7(3):1882–1904

Wright D, Rajalingam B, Karp JM, Selvarasah S, Ling Y, Yeh J, Langer R, Dokmeci MR, Khademhosseini A (2008) Reusable, reversibly sealable parylene membranes for cell and protein patterning. J Biomed Mater Res Part A 85(2):530–538

Yang SY, Ryu I, Kim HY, Kim JK, Jang SK, Russell TP (2006) Nanoporous membranes with ultrahigh selectivity and flux for the filtration of viruses. Adv Mater 18(6):709–712

Zhang Y, Fane A, Law A (2006) Critical flux and particle deposition of bidisperse suspensions during crossflow microfiltration. J Membr Sci 282(1–2):189–197